Shaker Pore Structure as Predicted by Annealed Atomic Simulation Using Symmetry and Novel Geometric Restraints

Pei-Kun Yang, Chyuan-Yih Lee, and Ming-Jing Hwang
Division of Structural Biology, Institute of Biomedical Sciences, Academia Sinica, Taipei 11529, Taiwan, Republic of China

ABSTRACT Recent studies making use of channel-blocking peptides as molecular calipers have revealed the architecture of the pore-forming region of *Shaker*-type potassium channels. Here we show that the low-resolution, experimentally derived geometric information can be incorporated as restraints within the context of an annealed molecular dynamics simulation to predict an atomic structure for the channel pore which, by virtue of restraints, conforms to the experimental evidence. The simulation is reminiscent of the computational method employed by nuclear magnetic resonance (NMR) spectroscopists to resolve solution structures of biological macromolecules, but in lieu of restraints conventionally derived from NMR spectra, novel restraints are developed that include side-chain orientation of amino acid residues and assumed symmetry of protein subunits. The method presented here offers the possibility of expanding cooperation between simulation and experiment in developing structural models, especially for systems such as ion channels whose three-dimensional structures may not be amenable to determination by direct methods at the present time.

INTRODUCTION

The membrane-inserting linker of the fifth and sixth transmembrane domain of *Shaker* channels is one of the most scrutinized of protein segments, having a large volume of experimental data illustrating how central this pore-forming sequence of ~20 amino acid residues, known as the "P region," is to the function of voltage-dependent ion channels (for a recent review, see Catterall, 1995). Its structure, however, has become more defined only within the past few years, as a result of several innovative experimental analyses. Among these, application of scanning mutagenesis and small reactive agents (Kürz et al., 1995; Lü and Miller, 1995; Pascual et al., 1995a; Gross and MacKinnon, 1996) reveals a non-alternating pattern of side-chain orientation for the P-region residues that cannot be discerned with a β-barrel structure (Bogusz et al., 1992; Durell and Guy, 1992), a model that until recently had been favored. Moreover, footprints of many critical residues of this domain have been obtained by independent research groups who took advantage of a complementary fit between the channel and its inhibitory peptide toxins which, with their structures known, serve as molecular calipers (Goldstein et al., 1994; Stampe et al., 1994; Hidalgo and MacKinnon, 1995; Aiyar et al., 1995; Lü and Miller, 1995; Ranganathan et al., 1996; Gross and MacKinnon, 1996; Naini and Miller, 1996; Naranjo and Miller, 1996). Collectively, these experiments sketch out a shallow vestibule of estimated dimensions for the outer mouth of the channel pore. These geometric data represent stringent requirements for computer models that have been useful in interpreting and hypothesizing structure-function relationships of ion channels in the absence of an experimental structure (e.g., Guy and Durell, 1994).

Structural predictions of membrane proteins on the one hand are unreliable due to a very small database of known structures, but on the other hand can benefit from a much-reduced conformational space in well-defined and usually homogeneous secondary structures of transmembrane domains. However, this advantage may not apply to K^+ or the closely related Na^+ and Ca^{2+} channels because increasing evidence points to an irregular loop structure for their ion-conducting pore lining, thus annotating a structural notion to the term "pore loops" (MacKinnon, 1995). Consequently, structural models of these channels (Bogusz et al., 1992; Durell and Guy, 1992; Bradley and Richards, 1993; Lipkind and Fozzard, 1994; Lipkind et al., 1995; Sansom and Kerr, 1995; Guy and Durell, 1995) have been largely the products of extensive maneuvers of interactive molecular graphics mingled with the modeler's discretion and/or presupposed secondary structures.

In principle the three-dimensional structure of a protein can be deduced without having to know the underlying physics of protein folding if enough structural information about the protein is available. This has been illustrated repeatedly in the increasing number of protein structures solved with nuclear magnetic resonance (NMR) methods (Gronenborn and Clore, 1994). In such structure determinations, hundreds to thousands of geometric restraints, mainly nuclear Overhauser effect (NOE) distances and J-coupling dihedral angles derived from NMR spectra, are required. Once sufficient restraints are assigned, the folded structure can be brought to light from an unfolded state by a computational procedure known as simulated annealing molecular dynamics (SA/MD) (e.g., Clore and Gronenborn, 1989).

In the present work we apply the same SA/MD method of NMR structure determination to the ion-conducting pore of

Received for publication 5 December 1996 and in final form 27 February 1997.

Address reprint requests to Dr. Ming-Jing Hwang, Institute of Biomedical Sciences, Academia Sinica, 128 Yen-chiou Yuan Rd., Sec. 2, Taipei 11529, Taiwan, ROC. Tel.: 886-2-789-9033; Fax: 886-2-785-3569; E-mail: mjhwang@ibms.sinica.edu.tw.

0006-3495/97/06/2479/11 $2.00

the *Shaker* channel. The usual NOE and J-coupling restraints of NMR structure determination are replaced by, among others of minor importance, 1) estimated pore radii, reported by peptide toxins, at a number of positions (residues) in the outer mouth of the pore; 2) side-chain orientations (with respect to the pore axis) as suggested by scanning mutagenesis studies; 3) assumed α-helical structure for the amino half of the P region; and 4) fourfold symmetry relationship of the four repeating subunits whose spatial assembly forms the pore. These restraints, especially the latter two, drastically reduce the conformational space of the polypeptide chain of the P region and, as presented below, allow structure convergence to a resolution of <3.5 Å in Cα coordinates from different simulation runs. By virtue of meeting the restraints, the resulting structure conforms to the vestibule architecture derived from recent experimental data. This is the first P-region model whose derivation is completely driven by an energy-based simulation employing extreme dynamical perturbations.

METHODS

SA/MD

The procedure of our SA/MD method is given in Table 1. In this procedure the MD was essentially carried out at a temperature of 1000 K, using a temperature annealing of 100 K per picosecond (ps) to change from and to 300 K at the beginning and the end of the simulation, respectively. By integrating over timesteps of 1 fs each, the simulation covered a period of ~45 ps for each structure run. A quartic-type, repulsive-only nonbonded potential (MSI, 95 release) similar to that of Nilges et al. (1988a) was used for the dynamics simulation, while in the last 2000 steps of energy minimization that followed the dynamics the potential was switched to the CVFF force field (MSI, 95 release) which includes both van der Waals (a Lennard-Jones type) and Coulomb interactions. Nonbond cutoff for the repulsive-only potential and CVFF is 3 Å and 9.5 Å, respectively. For the charge-charge interaction of CVFF, a dielectric constant of four times the distance ($4r$) was used. Throughout the simulation, including minimization, the added penalty functions of restraints were applied, whose force constants are given in Table 2.

The present protocol takes ~20 h per run on an SGI Indigo^2/R4400 machine for the present system. It is a modified implementation from the Discover molecular simulation package (MSI, 95 release) in which the original version was intended for solving solution structure of proteins with conventional restraint data of NMR. The basic rationale of this method is as follows. Initially, all the atoms of the system are allowed to move at a very high temperature (e.g., 1000 K) without being restricted by normal forces of the potential energy function. That is, the force field governing the equation of motion is scaled down significantly to be of minimal force. This has the effect of permitting atoms to break away from their bonding molecule and even pass through each other during the simulation, thereby facilitating the guidance of the initial structure to quickly comply with the imposed restraints, which are usually geometric relationships of individual atoms. Subsequently, the simulation is continued at this high temperature in concomitance with gradual increases in the scaled-down forces of the energy potential. This is the stage where most of the folding occurs and the structure takes its secondary and tertiary shapes, while at the same time the imposed restraints are maintained or improved. The system is then gradually quenched to the target temperature (e.g., room temperature) and equilibrated afterward with fully restored potential forces. This stage and energy minimizations that may follow allow further refinement of the folded structure and amino acid side chains to adopt low-energy conformations in the environment of a folded protein or protein complex. We note that the idea of combining drastic force field scaling and restraints to determine protein structures has been previously validated in cases where extensive interproton distances were used (Nilges et al., 1988a,b).

Restraints

Restraints are artificial forces devised to fold protein in simulation in a time scale (usually picosecond) manageable with present computing capability. Traditionally, they are usually formulated in terms of distances between atoms or conventionally defined internal coordinates (i.e., bond, bond angle, dihedral angle, etc.) of molecules. In the present work, we applied a tool control language (TCL) (Ousterhout, 1994) implemented in the Discover program (MSI, 95 release) to formulate nonconventional geometric restraints by which some of the recent biochemical data on K^+ channels can be incorporated into the simulation. The types of restraints and their parameters used in this work are summarized in Table 2.

Distance

The distance data imposed as restraints in the simulation are those derived from toxin footprinting by the group of Miller (Goldstein et al., 1994;

TABLE 1 SA/MD simulation protocol and scaling factors

	Prefolding	Main folding	Regulation	Cooling	Regulation	Minimization*
Temp (K)	300 → 1000	1000	1000	1000 → 300	300	
No. of steps#	9000	15000	10000	7000	5000	3000
Force field scaling factors§						
Covalent	0.000001	0.000001→	0.5→	1.0	1.0	1.0
Nonbond	0.001	0.001	0.001→	0.25→	1.0	1.0
Restraint scaling factors§						
Distance	0.001→	0.25→	1.0	1.0	1.0	1.0
Angle	0.001→	0.25→	1.0	1.0	1.0	1.0
Torsion	0	0.0001→	1.0	1.0	1.0	1.0
Chiral¶	0	0	0.03→	7.5→	30.0	1.0

*The repulsive-only potential used throughout the preceding dynamics was continued for 1000 steps and then switched to CVFF for the remaining 2000 steps.

#In the dynamics, 1 step equals 1 fs.

§Right arrow indicates that the initial value of the scaling factor is gradually increased, by either a geometric or arithmetic increment in each cycle (1 cycle = 1 ps), to the final value, which is shown in the next stage of simulation.

¶Chiral restraint was introduced at a relatively late stage, when most of the folding had been completed; early onset of chiral restraint would lead to highly strained structures.

TABLE 2 Geometric restraints imposed and results of the predicted structure

Distance (Å)				
Residue-to-pore axis				
residue		experiment*	restraint	predicted
F425		14–16 (~20)	14–22	20.1
K427		(15–20)	14–22	19.0
D431		14–17 (10–15) [12–15]	10–17	14.6
Y445		—	4–6	4.7
T449		4.5–7 (~5) [~4]	4–8	5.7
V438		[zone 1]	4–10	9.6
Residue-to-residue#				
residue 1	residue 2	experiment*	restraint	predicted
T449	D431	7–12	5–10§	9.9
D431	F425	4–8 (10–15)	4–15	12.5
D431	K427	(10–15)	4–15	6.3
Side-chain orientation¶				
inward ($\theta < 75°$): K427, S428, D431, W434, W435, V438, V443, Y445, D447, M448, T449				
outward ($\theta > 105°$): I429, A432, F433, A436, V437, G446				
violation in the predicted structure: D431($\theta = 75.8°$) and V443 ($\theta = 75.4°$)				
Spatial relationship‖				
residue 1				residue 2
S424		∨ & >		F425
F425		∨ & >		F426
F426		∨ & >		K427
K427		∨ & >		S428
V453		∨ & >		G452
G452		∨ & >		V451
V451		∨ & >		P450
P450		∨ & >		T449
K427		∨		D431
D431		∨		T449
Y445		∨		M440

Restraints: the quadratic force constants used for the restraint penalty functions are distance, 50 kcal/mol-Å^2; angle and dihedral angle, 200 kcal/mol-rad^2; chirality, 100 kcal/mol-rad^2. The ω angle representing peptide planarity is restrained to be within $\pm 160°$ for every residue of the P-region sequence simulated. Intra-helix restraints used for sequence 429 to 439 are: 1) distances between the carbonyl O of residue i and the amide H of residue i+4, to be within the range of 1.5 Å and 2.5 Å; 2) Ramachandran (ϕ, ψ) angles to be within ($-65° \pm 15°$, $-40° \pm 15°$); 3) for S428, the capping residue, its ϕ angle is restrained to be within $-130°$ and $-70°$, and ψ angle within 155° and 175°, based on a statistical observation (Harper and Rose, 1993).

Structure: the predicted structure is taken to be the average structure, as described in Table 3 and Fig. 3. Note that the only restraint violations in the predicted structure are two side-chain angle violations, which are quite small (<1°).

*The experimental data were taken from Chandy's group (Aiyar et al., 1995); and, in parentheses, from Miller's group; in brackets, from MacKinnon's group.

#For T449–D431, it is the distance between their side-chain geometric centers (see Fig. 1 *A*); for D431–F425 and D431–K427, it is the distance between their vertical depth within the pore, i.e., the distance between their "cCA" (see Fig. 1 *B*).

§A smaller upper bound is used because with it we achieved a better structural convergence in limited test runs.

¶In principle, 90° should be used to separate between inward and outward side-chain projections, but in practice we found a buffer of $\pm 15°$ is more discriminatory.

‖"∨" and ">" stand for an upper and outer position, respectively, in the pore (see Fig. 1 *B*).

Stampe et al., 1994; Lü and Miller, 1995; Naini and Miller, 1996; Naranjo and Miller, 1996), McKinnon (Hidalgo and MacKinnon, 1995; Ranganathan et al., 1996; Gross and MacKinnon, 1996), and Chandy (Aiyar et al., 1995) for residues at the extracellular entrance of a K^+ pore. As can be seen from Table 2, while consistent overall, variations in these data are evident up to several angstroms, which is likely due to a limitation on the precision of these experimental estimates as well as the fact that different members of the *Shaker* family were studied. To account for possible uncertainties, a larger range of distance values enclosing the experimental estimates was used (see, however, Table 2, §). This was done by introducing penalty functions of a one-sided or flat-bottom type to the energy equation of the simulation. Furthermore, since the experimental data refer only to residues and not to specific atoms, in these distance restraints each involved residue was represented by its geometric center (defined as a pseudoatom, Fig. 1 *A*), whose Cartesian coordinates were frequently updated to reflect any significant movement of the constitutive atoms during the simulation.

In contrast to the outer mouth of the pore, much less is known about the structure of the inner mouth. No specific distance data as above are available. However, since V438 was identified as one of the residues located within the central zone of the pore (Gross and MacKinnon, 1996), it was restrained to be at most 10 Å away from the pore axis in the simulation.

Side-chain orientation

As described in Fig. 1 *A*, by restraining on the value of the angle formed by 1) Cα (the apex atom), 2) centroid of Cα and its three symmetry-related equivalents, and 3) centroid of side-chain atoms, we can effectively "force"

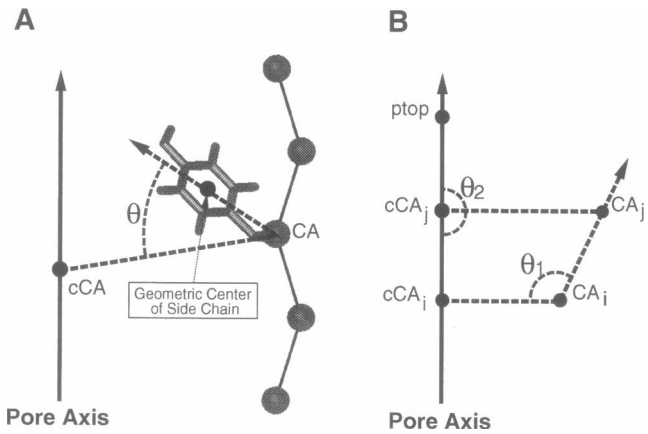

FIGURE 1 The angular geometric restraints devised for imposing (*A*) amino acid side-chain orientation, and (*B*) spatial relationship between two residues. "CA" denotes the α carbon of the interested residue, "cCA" is the geometric center of the four symmetry-related α carbons, each from one of the four P-region subunits, and "ptop" is a fixed point on the pore axis far above all the channel atoms. By requiring "θ" to be less (or greater) than 90° through a one-sided penalty function of a quadratic type, one can "force" a specific residue to project its side chain toward (or away from) the pore axis during the simulation. Similarly, by restraining "θ_1" to be greater than 90° and "θ_2" equal to 180°, one can "force" residue j to reside relatively outward and upward, respectively, within the pore than residue i does.

a residue to project its side chain either into or away from the pore lumen. This allows incorporation of the side-chain accessibility data determined by site-directed chemical modification studies. Residues with no or ambiguous experimental results were not subjected to the restraint.

α-Helix for the amino half of the P region

Circular dichroism measurements on synthetic peptides corresponding to segments of the *Shaker* P domain indicate that its amino half adopts a helical structure in hydrophobic environments (Peled and Shai, 1993). This is in accord with the pattern of solvent accessibility deduced from scanning mutagenesis analysis for a stretch of P-region residues spanning from K427 to V438 (Lü and Miller, 1995; Gross and MacKinnon, 1996). Furthermore, a helix N-capping sequence, S428-X-X-D, at the amino end of this stretch has been noted recently (Gross and MacKinnon, 1996). Taken together, it seems reasonable to assume this part of the pore loop adopts a helical conformation. Accordingly, in the simulation backbone dihedral angles and hydrogen bonds normal for a standard α-helix of a serine-capped configuration (Harper and Rose, 1993) were imposed as restraints to accelerate and maintain helix formation of this portion of the P domain (aa 428–439; the proposition that the helix terminates at residue 439 (Lü and Miller, 1995) was followed).

Fourfold symmetry

Supported by functional stoichiometry analysis (MacKinnon, 1991; MacKinnon et al., 1993) and electron microscopy imaging (Li et al., 1994), the four α subunits of K^+ channels are generally presumed to obey a fourfold symmetry centralized on the pore axis. To impose this symmetry we used a simple but apparently effective scheme in which a perfect fourfold symmetrized pore structure is regenerated during the simulation periodically by performing a symmetry operation on each of the four subunits in turn, and choosing the complex with lowest energy to continue the simulation (also see below for further discussion).

Relative spatial relationships

In the present work only the heart of the pore (*Shaker* sequence 424–453) was simulated, in part to keep the system computationally manageable. However, this leaves terminal residues at both ends of the P loop, i.e., residues upstream to 426 and downstream to 450, dangle in the dynamics simulation as most of them are not tied to any geometric restraints except symmetry. In order to prevent these projecting residues from folding back into the pore center, a relative orientational restraint was devised to force a residue to take a position that is relatively up and out (with respect to the pore axis) from its spatially preceding residue. As demonstrated in Fig. 1 *B*, this topological relationship, though without a specific geometric measure, can be simulated by imposing restraint on artificial angles whose formation is made possible by incorporating a distant pseudoatom which, unlike the side-chain pseudoatom described above, is fixed in space and on the pore axis throughout the simulation. This type of restraint is also applied to the spatial relationship of three important residues, K427, D431, and T449, the order of whose depth within the pore has been determined by their interactions with specific toxin residues (Naini and Miller, 1996). Additionally, using this type of restraint we place M440 in the intracellular side of Y445 to avoid undesirable topologies, which may turn up in the simulation due to lack of restraints on residues from 439 to 442. This assignment is consistent with the evidence that this part of the P region contributes to form the inner mouth of the pore (Yellen et al., 1991; Pascual et al., 1995a; Lü and Miller, 1995).

Others

In addition to the above, conventional restraints on ω angles (peptide bond rotation) and chiralities are also imposed. They were introduced as dihedral angle restraints.

RESULTS

Folding and subunit symmetry

Shown in Fig. 2 are several snapshots of the pore structure taken at representative stages of the simulation, and time series of the root-mean-squares deviation (rmsd) from perfect fourfold symmetry for a typical successful run. As can be seen, starting from a fully extended but formed into a "U"-shaped polypeptide chain, the four P-region segments are efficiently guided to fold into a highly structured assembly whose deviation from a perfect fourfold rotational symmetry is reset repeatedly, at each picosecond mark of the simulation. With the resetting scheme, additional perturbation to the simulated structure at early stages of the simulation is introduced, but as the simulation goes on and the structure becomes folded, the perturbation dies out quickly and produces merely a noise of <0.5 Å rmsd at the end. To force or maintain a protein subunit symmetry in a classical molecular simulation, alternatively one can devise geometric restraints such as inter-subunit distances (Nilges, 1993) or angular relationships (Yang and Hwang, unpublished observations), but the present resetting scheme appears to work well, and can do without the extra restraints that may stifle the system inadvertently.

Structural convergence

The simulation protocol as described in Table 1 was repeated 32 times; each time a different Boltzmann distribu-

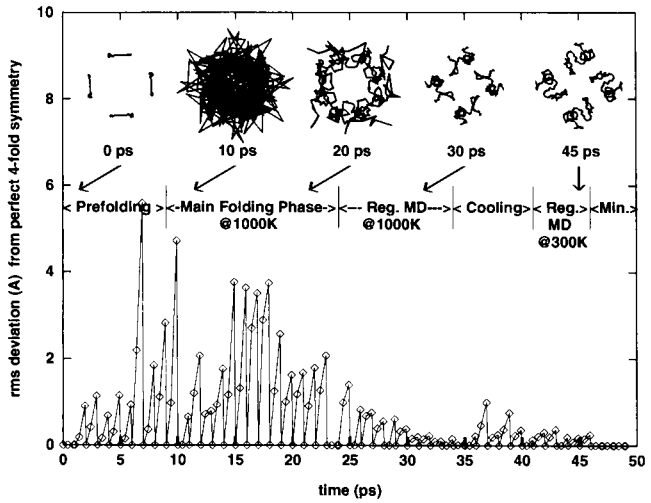

FIGURE 2 Snapshots of the pore structure, shown by traces of backbone atoms and viewed from the pore top, and time series of its deviation from perfect fourfold symmetry, from a typical successful run. The arrows point approximately to the time frame at which the corresponding structure was extracted. The initial structure, at 0 picosecond (ps), is a "U"-shape, but otherwise a fully extended P segment for each subunit, where its central four or six residues compose the bottom of the U. The structure at 10 ps was scaled down considerably in size so as to be compatible with the others, as shown. Throughout the simulation, at each picosecond mark the assembly structure was adjusted to maintain fourfold symmetry, which gives rise to the reset of the deviation.

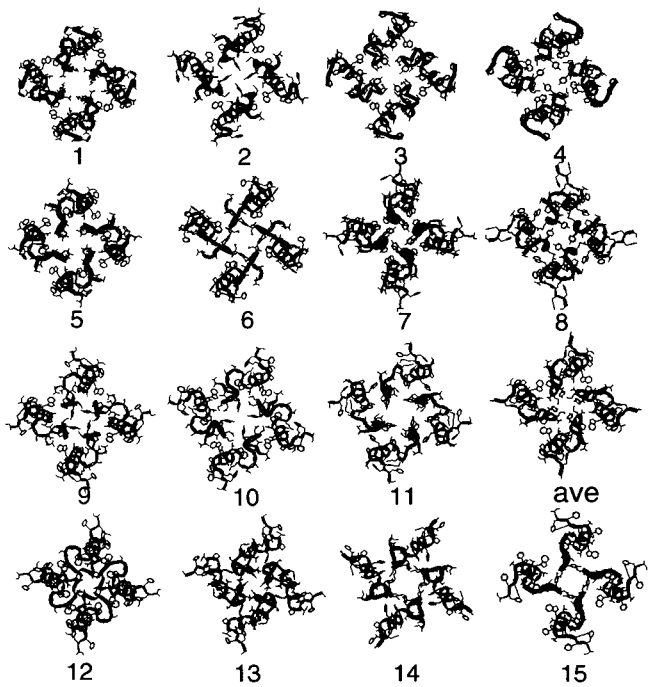

FIGURE 3 An extracellular view of all the pore structures that are successfully converged. The structure labeled *ave* is the average structure of the first 11, obtained through coordinates averaging and energy minimization. The last four structures are somewhat unique because they deviate slightly from the rest in the overall fit of the superimposed Cα coordinates.

tion of initial atomic velocities was used. It follows that the trajectory of each and every simulation run is unique. Of the 32 attempts, 15 were considered successful based on their significantly lower energy (50% to severalfold) and negligible restraint violations (see below), and consequently they were selected for further analysis. Many of the unsuccessful runs resulted in a highly distorted structure, indicating there is still room for improving the simulation protocol. When superimposed on each other, the resulting pair rmsd in the Cα coordinates of the 15 successfully derived structures (Fig. 3) show that 4 of them have an averaged pair rmsd >4.0 Å (data not shown), while the remaining 11 structures are, on the average, within 3.2 ± 0.4 Å of each other, and 2.3 ± 0.5 Å to their averaged structure (see Table 3). In Fig. 4 the 11 structures are superimposed together, showing a clearly convergent pore structure. Furthermore, 2 of the 11 structures were simulated with a slightly different initial structure, where the bottom of the "U" consists of 6 residues instead of the normal 4 used for the other runs. This may indicate that the final structure is fairly insensitive to the exact shape of the initial structure used. However, a rigorous test would be to use a randomized initial structure (Nilges et al., 1988b), but this was not pursued because preliminary test runs indicated that initially intertwined P-region segments are very difficult to untangle with the present simulation protocol, due most probably to the symmetry relationship demanded here.

Restraint violation

All the successful runs have essentially negligible violations on the restraints imposed, which is typified in the results given in Table 2 of the average structure derived from the above-mentioned 11 successful runs (Table 3 and Fig. 3). In fact, this satisfactory result extends to the four structures which, although also successfully converged, deviate somewhat from the others as discussed above. As may be seen in Fig. 3, in an overview they do not appear to vary from the rest, but some subtle yet distinctive features can be noted. For instance, in structure 13 the four helices are visually more twisted and spiraled, and in structure 12 the carboxyl end of the P loop appears to cross over the helix. Since they are compatible with the 11 more homogeneous structures in both the total energy and restraint violations, they remain viable candidates for the pore structure. These results may suggest that at least one piece of key discriminatory information to resolve this problem is missing in the present set of restraints.

DISCUSSION

Features of the predicted K+ pore structure

The predicted structure, which is taken to be the average structure (Fig. 3), is depicted in two stereo views, from top and from side, in Fig. 5 *A* and *B*, respectively. In the latter,

TABLE 3 Pairwise rms deviations (in Å) in the Cα coordinates of the final pore structure resulting from the eleven successful runs

Run no.	2	3	4	5	6	7	8	9	10	11	ave	to ave str*
1	3.4	3.0	2.6	2.2	2.5	3.4	2.9	3.3	3.0	3.0	2.9	2.0
2		3.3	3.5	3.5	3.3	3.9	3.7	4.3	3.3	3.7	3.6	2.8
3			3.1	3.3	3.0	4.2	3.6	3.8	3.2	3.3	3.4	2.7
4				2.7	3.0	3.3	2.5	3.1	2.5	3.2	3.0	2.2
5					2.3	3.2	2.4	3.0	3.0	3.2	2.9	2.0
6						3.3	2.9	3.1	2.8	3.1	2.9	1.8
7							2.3	2.7	4.0	4.0	3.4	2.7
8								2.5	3.4	3.6	3.0	2.2
9									3.5	3.8	3.3	2.7
10										2.3	3.1	2.1
11											3.3	2.6
Average											3.2 ± 0.4	2.3 ± 0.5

*The average structure was obtained by taking the mean of the coordinates of the 11 structures, and then energy minimized under the same set of restraints employed in the simulation.

residues that are involved in the distance restraints (Table 2) imposed in the simulation are labeled. As may be seen, the structure of the outer mouth can indeed be described as a shallow vestibule that narrows rapidly at the center of the pore, a result that attests to the effectiveness of the present simulation approach and the restraints imposed. In addition, as might be expected for a fourfold symmetrical architecture, the shape of the pore structure is that of a square when viewed through the symmetry axis, with each of the four P-region segments contributing equally to the assembly. Whereas these have been envisioned based on the results of toxin footprinting (e.g., Miller, 1995; Gross and MacKinnon, 1996), the atomic model reveals abundant new features as well as unprecedented details of the pore structure. The following are most notable.

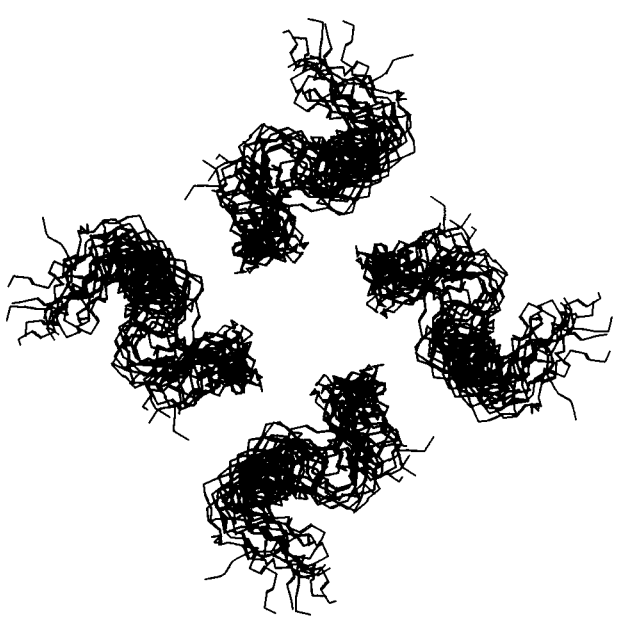

FIGURE 4 Stick representations of the 11 convergent and more homogeneous pore structures (see Fig. 3), as superimposed on their average structure.

First, the P-region segment, in a structure of helix-turn-loop type, orients toward the pore center in such a way that both the C-terminal loop and the N-terminal helix contribute together to make up the pore lumen. Furthermore, helices of adjacent subunits do not make a direct contact with each other; they are instead interposed by the winding loop, which extrudes from the intracellular side. In such an arrangement, of particular interest is regarding the two tryptophans, W434 and W435, which are found to reside in the pore deeper than T449 and D431, and yet their side chains are apparently accessible from the pore outside simply because the loop is in some manner twisted away at the right position to accommodate their exposure. The two tryptophans are perhaps the most difficult residues to model in terms of satisfying the side-chain accessibility data (Lü and Miller, 1995; Gross and MacKinnon, 1996), because from a structural viewpoint their solvent access could be easily blocked by some of the loop residues that have been shown to line the narrowest region of the channel. With this model access W434 and W435 is effectively achieved, so is the agreement with the observation that these two residues are not among the channel residues shown to interact strongly with channel-blocking toxins, a result that would be expected for a pore lumen residue located deeper than T449 and D431, and not as close to the pore axis as D447 or Y445.

Second, in the predicted structure, the conformation of residues at the carboxyl end (aa 443–451) would all be extended if it were not for G444, D447, and T449. It follows that in this region no consecutive three residues of β-strand conformation exist, giving the loop an irregular shape. The backbone dihedral angles for G444 and D447 are similar, both having a Ramachandran (Φ, Ψ) angle in the neighborhood of ($-120°$, $-120°$), while T449 takes a right-handed helical conformation with a (Φ, Ψ) angle very close to (65°, 45°). These three residues are thus responsible for the twisting and bending of the extruding loop in the predicted structure. However, we note that, although the overall shape of the loop structure is fairly homologous among the con-

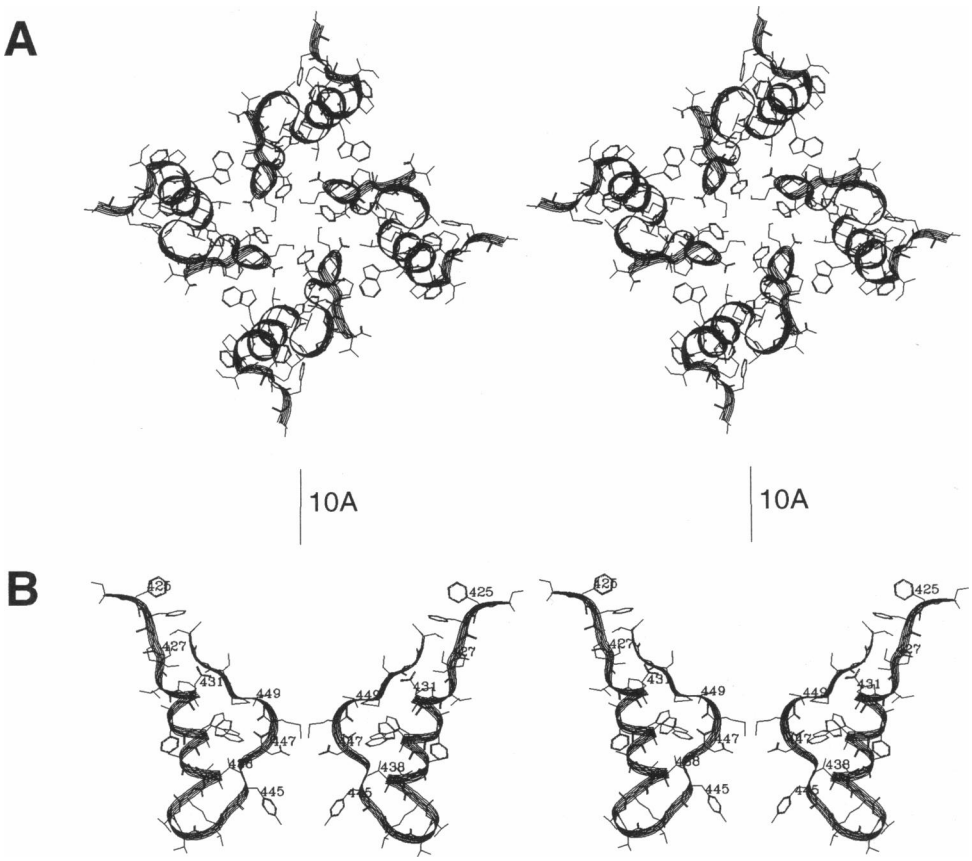

FIGURE 5 Two stereo pictures of the predicted *Shaker* pore structure (the *ave* structure shown in Fig. 3). (*A*) a top view from outer mouth, and (*B*) a cross-section view of two opposing subunits with residues involved in distance restraints labeled.

vergent pore structures, there is considerable variation in the local conformations, and thus (Φ, Ψ) angles of the loop residues, as may be seen from Fig. 4. The cause of the variation may be attributed to insufficient restraints or, alternatively, a flexible loop structure. The implication of conformational flexibility for the pore-lining loop is likely to confer functional significance, as it is in line with a recent study suggesting that three residues in the outer mouth, M448, T449, and P450, rearrange their side-chain orientations during a gating event (Liu et al., 1996). We note also that none of the residues of the predicted structure falls in the disallowed regions of the Ramachandran plot when checked by the program PROCHECK (Laskowski et al., 1993), indicating that the conformational feasibility of the predicted structure is sustainable.

Third, it can be seen that residues from Y445 to T449 compose the narrowest portion of the channel where the four subunits meet (Fig. 5). This is a direct consequence of the distance restraints imposed (Table 2). The importance of T449 or its equivalents in other K^+ channels to the blockade of the extracellular agent tetraethylammonium (TEA) has been extensively documented (MacKinnon and Yellen, 1990; Kavanaugh et al., 1991; Heginbotham and MacKinnon, 1992; Pascual et al., 1995b). The conclusion appears to be unanimous in placing this residue at ~5–8 Å from the pore axis (Heginbotham and MacKinnon, 1992; Kavanaugh et al., 1992; Aiyar et al., 1995; Naranjo and Miller, 1996), which is, as expected, satisfied in the predicted structure. The position of Y445 restrained in this work (Table 2) is admittedly an assumption, but nevertheless one based on several lines of experimental evidence: 1) Cysteine accessibility analysis from both sides of the pore shows that residues at the *Shaker* D447 and V443 equivalents of Kv2.1 are exposed at outer and inner mouths of the channel, respectively, giving rise to the suggestion that the GYG triplet, which is highly conserved among voltage-gated K^+ channels, lines the narrowest part of the ion conduction pathway (Pascual et al., 1995a). 2) A pair of mutants, one on K27 of Agitoxin2 and the other on Y445 of the channel, are shown to be functionally coupled, in a unique fashion that their interaction depends on K^+ concentration (Ranganathan et al., 1996). Upon channel binding, K27, a residue conserved throughout the scorpion toxin family, is thought to project its ϵ-amino group into the pore center at a position very close to the fourfold axis of symmetry. Indeed, the localization of K27 had provided a key basis for using toxins to map out the channel structures (Miller, 1995). 3) Using silver as a probe, it was found that the side chain of Y445 is exposed to the aqueous pore, but that of G446 is not (that of G444 is not known) (Lü and Miller, 1995).

A consequence of the distance and side-chain orientation restraints imposed on Y445 (Table 2) is the formation of a closely packed tyrosine quartet (see Fig. 5 *A*), a configuration that had also been proposed before (Lee, 1992; Bradley

and Richards, 1993). Interestingly, as can be seen from Fig. 5, a cavity along the ion permeation pathway near the pore center is encapsulated by four YGDM quartets, each from one of the four loops, with Y445 inclining its phenol ring toward the intracellular side, G446 swinging away to make room for the cavity, and D447 and M448 defining the upper bound of the cavity. This cavity makes an ideal cation-binding site since it is surrounded by abundant negative charges arising not only from the acidic residue of D447, but from the carbonyl group of G446, as well as the hydroxyl group and aromatic π electrons of Y445. Furthermore, extracellular entry to this site would be regulated by residues carboxyl-terminal to M448, T449 in particular, for its closeness to the pore axis. As peculiar as it might seem, this intriguing structural moiety finds support in results from a recent study on external Ba^{2+} block in *Shaker* channels (Hurst et al., 1996). In that study it was concluded that external Ba^{2+} binding to a K^+ site must overcome an access barrier imposed by T449, and D447 contributes to that site. In another and independent experiment, a binding site for K^+ ions in the neighborhood of Y445 is also implicated (Ranganathan et al., 1996).

Another interesting feature for this portion of the pore loop is the location of M448, which is predicted to be very close to the pore axis, in fact closer than T449 (Fig. 5 *B*). This prediction is consistent with the experimental evidence of the intersubunit cross-link of M448C channels (Gross and MacKinnon, 1996; Liu et al., 1996), but not with a data derived from functional zoning analysis (Gross and MacKinnon, 1996). However, the latter is difficult to reconcile with the topology of the pore loop and explanations for the inconsistent experimental result have been proposed (Gross and MacKinnon, 1996). Among those explanations, the suggestion that toxin may induce change in the local environment of the binding site is in a favorable concert with the conformational flexibility of the pore loop discussed above.

Fourth, each of the four helices occupies a corner of the square-shaped pore structure, and together they form a left-handed four-helix bundle (Fig. 5 *A*). These helices have a crossing angle to the pore axis of 14.5° and a tilt angle of 20.8°. However, unlike the solution helix bundles (Harris et al., 1994), they do not pack against each other, as noted above, though presumably they will interact with some of the other transmembrane domains of the channel, which are not treated in this work. The tilt angle is a result of the four helices narrowing downward into the inner side of the channel. It has been suggested that such an arrangement of channel helices can generate a macrodipole to attract cations into the pore (Gross and MacKinnon, 1996). More significantly, an electrostatic-surface calculation (data not shown) shows that the pore is essentially acidic, contributed primarily by the inward-projecting, negatively charged side chains of D431s and D447s. These results provide strong support for the feasibility of the predicted structure as a cation channel. Two different mechanisms, π face (Kumpf and Dougherty, 1993; Dougherty, 1996) and oxygen cage (Miller, 1993), have been proposed for the potassium selectivity and cation-amino acid interaction in ion channels. Our predicted structure shows that a mixture of both mechanisms is also feasible, and that by arranging the otherwise hydrophobic P-region residues and their side chains in a specific way, an effective cation channel can be formed.

Fifth, as mentioned above, experimentally the geometric positions of the inner mouth residues are much less certain than their counterparts at the outer mouth. As a result, the simulation-derived structure for this region is likely to be less certain as well. Nevertheless, the residues at positions 438, 440, 441, and 443, which have been shown to affect internal TEA blocking (see, e.g., a review by Joho, 1992), appear to be all accessible in the inner mouth of the predicted structure (see Fig. 5 *B*). Unlike T449, whose interaction with external TEA has been shown to involve all four subunits (Kavanaugh et al., 1992; Heginbotham and MacKinnon, 1992; Naranjo and Miller, 1996), to our knowledge this simultaneous interaction with multi-subunits has not been demonstrated for any of the internal TEA-interacting residues. Therefore, there is no basis at present to impose small-pore radii on these inner mouth residues, despite the evidence that they may interact with TEA. The only distance restraint applied to these residues in the simulation is a conservative 10-Å pore radius as an upper bound for V438 (see Table 2), which is based on the zoning assignment of Gross and MacKinnon (1996). One inconsistency does arise in the intracellularly inclined phenol ring of Y445, because if the predicted structure remains unchanged for its cysteine mutant, this residue would be readily accessible for reaction with sulfhydryl reagents applied from the intracellular side, a result not supported by experimental data (Pascual et al., 1995a). However, the void created by the cavity located immediately above Y445 (see above discussion) could easily accommodate an inverted, extracellularly projecting Y445, and such a ring inversion may induce contraction of neighboring residues such as V443, thereby creating a new cavity formed by, for example, Y445, G444, and V443 (each of them has four copies), and protecting Y445 and the residues external to it from an intracellular access. An extended implication of this cavity migration is a dynamic and modulated mechanism for transporting ions through a narrow passage in the channel (i.e., ions jump from one cavity to the next), and also for greatly reducing the separation between intracellular and extracellular surfaces of the pore. In supporting this hypothesis, for the former there is a recent report of barriers to Mg^{2+} movement created by residues at a position equivalent to *Shaker* V443 (Harris and Isacoff, 1996); for the latter there are data showing electrostatic repulsion between external and internal TEA ions (Newland et al., 1992).

Sixth, the height of the predicted pore structure, as measured from the floor of the extracellular surface (i.e., T449 and D431) to the loop turn connecting both halves of the P segment, is ~18 Å (see Fig. 5 *B*). This means that within the membrane, plenty of space will be available for components adjacent to the P region to contribute to the cytoplasmic part of the pore. Indeed, recent experiments have shown that

residues located in the loop between the fourth and fifth transmembrane segments (Slesinger et al., 1993) and in the cytosolic half of the sixth segment (Choi et al., 1993; Kirsch et al., 1993; Lopez et al., 1994; Taglialatela et al., 1994) interact with intracellular ions and blocking agents of K^+ channels.

Critique of the method and the derived structure

Despite the efforts made to follow closely the spirit and essence of NMR structure determination, there are still a number of assumptions and uncertainties intrinsic in the present simulation, which implies that the predicted pore structure must be labeled as a "theoretical model."

First, and perhaps the most drastic simplification of all, the simulated pore structure represents only a truncated domain of an intact channel. The surrounding transmembrane segments, especially the two linked by the pore loop, should contribute significantly to shape the pore structure as well as play a critical role in its stability. Indeed, the stability of the predicted pore structure was maintained by the restraints imposed; without them the structure lost its pore form in prolonged simulations (data not shown). Although the experimentally derived restraints have implicitly harbored some contributions from the left-out segments, including their interactions explicitly in the modeling is clearly more desirable. There should be no technical difficulties to extend the present simulation to include the surrounding segments (apart from the computational cost that would increase greatly), but for a simulation to be as objective one would need to know how these segments are positioned relative to one another, and to the pore loop, and how the individual segments are orientated with respect to the pore axis. To this end we are excited that data of this sort, already abundant for lactose permease (see, e.g., Kaback et al., 1994), are beginning to emerge for voltage-gated ion channels as well (e.g., Choe et al., 1995).

Second, unlike a typical NMR structure, which must satisfy numerous restraints, the convergence achieved on Cα atoms of the present model is primarily a result of the strictly imposed subunit symmetry and an α-helical segment; both, although well-based, are nonetheless propositions for which an indisputable confirmation awaits X-ray or NMR-derived structures. Moreover, the exact residue at which the assumed helix begins and ends is also unclear. In fact, the assumption of S428-capping excludes residue K427 as a part of the helix, whereas the solvent accessibility data suggest that it is a helix residue. However, we note that in the predicted structure the long lysine side chain adopts a folded conformation, and thereby can still satisfy the inward side-chain projection concluded for this residue. Adding to these uncertainties is the fact that the toxin-mapped distance data critical to the present simulation are only crude estimates; they are mainly intended to profile the pore structure, and not to produce the kind of resolution we hope to achieve here. In addition, subsequent to the completion of this work, we became aware that an agreement was reached between two recent studies in orienting Agitoxin2 (Ranganathan et al., 1996) and charybdotoxin (Naini and Miller, 1996) within the pore, respectively. Though not explicitly reported by these authors, the new toxin orientation implies that a refined set of distance data different from the original estimates can be deduced. The differences are expected to be small for residues close to the pore center, to which K27 of the toxin projects, but could be significant for those far away—a geometric consequence due to the downward narrowing nature of the outer mouth. Thus, for example, our own estimate for the pore radius of F425 in the new orientation is 10–16 Å, which is a bit smaller than the original estimates, 14–16 Å or ~20 Å, and the resulting prediction, 20.1 Å (see Table 2). The work of Ranganathan et al. (1996) also provided additional distance data for D447, M448, and V451, that were absent in the present restraints. The data on V451 would be more valuable to the simulation than the other two, because, like F425, V451 is a residue located farther away from the pore's converging point. Work to investigate the extent to which the new set of distance data will change the simulation-resulted pore structure presented above is currently in progress.

In summary, we have developed a novel simulation approach through which an atomic model for the structure of the *Shaker* pore can be derived. This model yields a wealth of structural details, which are scrutinized and shown to be in good agreement with considerable existing experimental data. Equally significant is that this novel approach represents a means to incorporate structural data of low resolution or indirect deduction into energy-driven atomic simulations, and, for the automated nature, refinement to fit new experimental data will be straightforward. As the structure of K^+ pore continues to be characterized by experimental data with increasing details, one can hope to close the gap between the confidence level that one normally exerts on an NMR structure and a structure derived using the present methodology. Many of the restraint techniques developed here, such as subunit symmetry, side-chain orientation, and non-specific spatial relationship, should also find wide applications in other molecular systems.

A generous supply of computing time by the National Center for High-Performance Computing is acknowledged.

This work was supported by Grants NSC 85-2113-M-001-011 and NSC 86-2314-B-001-035 from the National Science Council of Taiwan.

REFERENCES

Aiyar, J., J. M. Withka, J. P. Rizzi, D. H. Singleton, G. C. Andrews, W. Lin, J. Boyd, D. C. Hanson, M. Simon, B. Dethlefs, C.-L. Lee, J. E. Hall, G. A. Gutman, and K. G. Chandy. 1995. Topology of the pore-region of a K^+ channel revealed by the NMR-derived structures of scorpion toxins. *Neuron.* 15:1169–1181.

Bogusz, S., A. Boxer, and D. D. Busath. 1992. A SS1-SS2 β-barrel structure for the voltage-activated potassium channel. *Protein Eng.* 5:285–293.

Bradley, J. C., and W. G. Richards. 1993. Potassium channels: a computer prediction of structure and selectivity. *Protein Eng.* 7:859–862.

Catterall, W. A. 1995. Structure and function of voltage-gated ion channels. *Annu. Rev. Biochem.* 64:493–531.

Choe, S., C. F. Stevens, and J. M. Sullivan. 1995. Three distinct structural environments of a transmembrane domain in the inwardly rectifying potassium channel ROMK1 defined by perturbation. *Proc. Natl. Acad. Sci. USA.* 92:12046–12049.

Choi, K. L., C. Mossman, J. Aubè, and G. Yellen. 1993. The internal quaternary ammonium receptor site of *Shaker* potassium channels. *Neuron.* 10:533–541.

Clore, G. M., and A. M. Gronenborn. 1989. Determination of three-dimensional structures of proteins and nucleic acids in solution by nuclear magnetic resonance spectroscopy. *CRC Crit. Rev. Biochem. Mol. Biol.* 24:479–564.

Dougherty, D. A. 1996. Cation-π interactions in chemistry and biology: a new view of benzene, Phe, Tyr, and Trp. *Science.* 271:163–168.

Durell, S. R., and H. R. Guy. 1992. Atomic scale structure and functional models of voltage-gated potassium channels. *Biophys. J.* 62:238–250.

Goldstein, S. A. N., D. J. Pheasant, and C. Miller. 1994. The charybdotoxin receptor of a *Shaker* K^+ channel: peptide and channel residues mediating molecular recognition. *Neuron.* 12:1377–1388.

Gronenborn, A. M., and G. M. Clore. 1994. Where is NMR taking us? *Proteins Struct. Funct. Genet.* 19:273–276.

Gross, A., and R. MacKinnon. 1996. Agitoxin footprinting the *Shaker* potassium channel pore. *Neuron.* 16:399–406.

Guy, H. R., and S. R. Durell. 1994. Using homology in modeling the structure of voltage-gated ion channels. *In* Molecular Evolution of Physiological Processes. D. Fambrough, editor. The Rockefeller Univ. Press, New York. 197–212.

Guy, H. R., and S. R. Durell. 1995. Structural models of Na^+, Ca^{2+}, and K^+ channels. *In* Ion Channels and Genetic Diseases, D. C. Dawson and R. A. Frizzell, editors. The Rockefeller Univ. Press, New York. 1–16.

Harper, E. T., and G. D. Rose. 1993. Helix stop signals in proteins and peptides: the capping box. *Biochemistry.* 32:7605–7609.

Harris, N. L., S. R. Presnell, and F. E. Cohen. 1994. Four helix bundle diversity in globular proteins. *J. Mol. Biol.* 236:1356–1368.

Harris, R. E., and E. Y. Isacoff. 1996. Hydrophobic mutations alter the movement of Mg^{2+} in the pore of voltage-gated potassium channels. *Biophys. J.* 71:209–219.

Heginbotham, L., and R. MacKinnon. 1992. The aromatic binding site for tetraethylammonium ion on potassium channels. *Neuron.* 8:483–491.

Hidalgo, P., and R. MacKinnon. 1995. Revealing the architecture of a K^+ channel pore through mutant cycles with a peptide inhibitor. *Science.* 268:307–310.

Hurst, R. S., L. Toro, and E. Stefani. 1996. Molecular determinants of external barium block in *Shaker* potassium channels. *FEBS Lett.* 388: 59–65.

Joho, R. H. 1992. Towards a molecular understanding of voltage-gated potassium channels. *J. Cardiovasc. Electrophysiol.* 3:589–601.

Kaback, H. R., S. Frillingos, H. Jung, K. Jung, G. G. Privè, M. L. Ujwal, C. Weitzman, J. Wu, and K. Zen. 1994. The lac permease meets Frankenstein. *J. Exp. Biol.* 196:183–195.

Kavanaugh, M. P., R. S. Hurst, J. Yakel, M. D. Varnum, J. P. Adelman, and R. A. North. 1992. Multiple subunits of a voltage-dependent potassium channel contribute to the binding site for tetraethylammonium. *Neuron.* 8:493–497.

Kavanaugh, M. P., M. D. Varnum, P. B. Osborne, M. J. Christie, A. E. Busch, J. P. Adelman, and R. A. North. 1991. Interaction between tetraethylammonium and amino acid residues in the pore of cloned voltage-dependent potassium channels. *J. Biol. Chem.* 266:7583–7587.

Kirsch, G. E., C.-C. Shieh, J. A. Drewe, D. F. Vener, and A. M. Brown. 1993. Segmental exchanges define 4-aminopyridine binding and the inner mouth of K^+ pores. *Neuron.* 11:503–512.

Kumpf, R. A., and D. A. Dougherty. 1993. A mechanism for ion selectivity in potassium channels: computational studies of cation-π interactions. *Science.* 261:1708–1710.

Kürz, L. L., R. D. Zühlke, H.-J. Zhang, and R. H. Joho. 1995. Side-chain accessibilities in the pore of a K^+ channel probed by sulfhydryl-specific reagents after cysteine-scanning mutagenesis. *Biophys. J.* 68:900–905.

Laskowski, R. A., M. W. MacArthur, D. S. Moss, and J. M. Thornton. 1993. PROCHECK: a program to check the stereochemical quality of protein structures. *J. Appl. Cryst.* 26:283–291.

Lee, C. Y. 1992. A possible biological role of the electron transfer between tyrosine and tryptophan: gating of ion channels. *FEBS Lett.* 299:119–123.

Li, M., N. Unwin, K. A. Stauffer, Y.-N. Jan, and L. Y. Jan. 1994. Images of purified *Shaker* potassium channels. *Curr. Biol.* 4:110–115.

Lipkind, G. M., and H. A. Fozzard. 1994. A structural model of the tetrodotoxin and saxitoxin binding site of the Na^+ channel. *Biophys. J.* 66:1–13.

Lipkind, G. M., D. A. Hanck, and H. A. Fozzard. 1995. A structural motif for the voltage-gated potassium channel pore. *Proc. Natl. Acad. Sci. USA.* 92:9215–9219.

Liu, Y., M. E. Jurman, and G. Yellen. 1996. Dynamic rearrangement of the outer mouth of a K^+ channel during gating. *Neuron.* 16:859–867.

Lopez, G. A., Y. N. Jan, and L. Y. Jan. 1994. Evidence that the S6 segment of the *Shaker* voltage-gated K^+ channel comprises part of the pore. *Nature.* 367:179–182.

Lü, Q., and C. Miller. 1995. Silver as a probe of pore-forming residues in a potassium channel. *Science.* 268:304–307.

MacKinnon, R. 1991. Determination of the subunit stoichiometry of a voltage-activated potassium channel. *Nature.* 500:232–235.

MacKinnon, R. 1995. Pore loops: an emerging theme in ion channel structure. *Neuron.* 14:889–892.

MacKinnon, R., R. W. Aldrich, and A. W. Lee. 1993. Functional stoichiometry of *Shaker* potassium channel inactivation. *Science.* 262:757–759.

MacKinnon, R., and G. Yellen. 1990. Mutations affecting TEA blockade and ion permeation in voltage-activated K^+ channels. *Science.* 250: 276–279.

Miller, C. 1993. Potassium selectivity in proteins: oxygen cage or in the face? *Science.* 261:1692–1693.

Miller, C. 1995. The charybdotoxin family of K^+ channel-blocking family. *Neuron.* 15:5–10.

Naini, A. A., and C. Miller. 1996. A symmetry-driven search for electrostatic interaction partners in charybdotoxin and a voltage-gated K^+ channel. *Biochemistry.* 35:6181–6187.

Naranjo, D., and C. Miller. 1996. A strongly interacting pair of residues on the contact surface of charybdotoxin and a *Shaker* K^+ channel. *Neuron.* 16:123–130.

Newland, C. F., J. P. Adelman, B. L. Tempel, and W. Almers. 1992. Repulsion between tetraethylammonium ions in cloned voltage-gated potassium channels. *Neuron.* 8:978–982.

Nilges, M. 1993. A calculation strategy for the structure determination of symmetric dimers by ^1H NMR. *Proteins Struct. Funct. Genet.* 17: 297–309.

Nilges, M., G. M. Clore, and A. M. Gronenborn. 1988a. Determination of three-dimensional structures of proteins from interproton distance by hybrid distance geometry-dynamical simulated annealing calculations. *FEBS Lett.* 229:317–324.

Nilges, M., G. M. Clore, and A. M. Gronenborn. 1988b. Determination of three-dimensional structures of proteins from interproton distance by dynamical simulated annealing from a random array of atoms. *FEBS Lett.* 239:129–136.

Ousterhout, J. K. 1994. Tcl and the Tk Toolkit. Addison-Wesley Publishing, Reading, Massachusetts.

Pascual, J. M., C.-C. Shieh, G. E. Kirsch, and A. M. Brown. 1995a. K^+ pore structure revealed by reporter cysteines at inner and outer surfaces. *Neuron.* 14:1055–1063.

Pascual, J. M., C.-C. Shieh, G. E. Kirsch, and A. M. Brown. 1995b. Multiple residues specify external tetraethylammonium blockade in voltage-gated potassium channels. *Biophys. J.* 69:428–434.

Peled, H., and Y. Shai. 1993. Membrane interaction and self-assembly within phospholipid membranes of synthetic segments corresponding to the H-5 region of the *Shaker* K^+ channel. *Biochemistry.* 32:7879–7885.

Ranganathan, R., J. H. Lewis, and R. MacKinnon. 1996. Spatial localization of the K^+ channel selectivity filter by mutant cycle-based structure analysis. *Neuron.* 16:131–139.

Sansom, M. S. P., and I. D. Kerr. 1995. Transbilayer pores formed by β-barrels: molecular modelling of pore structures and properties. *Biophys. J.* 69:1334–1343.

Slesinger, P. A., Y. N. Jan, and L. Y. Jan. 1993. The S4–S5 loop contributes to the ion-selective pore of potassium channels. *Neuron*. 11:739–749.

Stampe, P., L. Kolmakova-Partensky, and C. Miller. 1994. Intimations of K^+ channel structure from a complete functional map of the molecular surface of charybdotoxin. *Biochemistry*. 33:443–450.

Taglialatela, M., M. S. Champagne, J. A. Drewe, and A. M. Brown. 1994. Comparison of H_5, S_6, and H_5-S_6 exchanges on pore properties of voltage-dependent K^+ channels. *J. Biol. Chem.* 269:13867–13873.

Yellen, G., M. E. Jurman, T. Abramson, and R. MacKinnon. 1991. Mutations affecting internal TEA blockade identify the probable pore-forming region of a K^+ channel. *Science*. 251:939–942.